molecules

MDPI

Article

A Waterborne Epoxy Composite Coating with Smart Corrosion Resistance Based on 2-Phenylbenzimidazole-5-sulfonic Acid/Layered Double Hydroxide Composite

Caiyou Ding [1,†], Jiongxin Wu [2,†], Yuan Liu [1,*], Xinxin Sheng [2,*], Xiaoling Cheng [1], Xiaoyan Xiong [3] and Wenlin Zhao [4]

[1] Guangdong Provincial Key Laboratory of Plant Resources Biorefinery, School of Chemical Engineering and Light Industry, Guangdong University of Technology, Guangzhou 510006, China
[2] Guangdong Provincial Key Laboratory of Functional Soft Condensed Matter, School of Materials and Energy, Guangdong University of Technology, Guangzhou 510006, China
[3] Center for Industrial Analysis and Testing, Guangdong Academy of Sciences, Guangzhou 510650, China
[4] GCH Technology Co., Ltd., Guangzhou 510540, China
* Correspondence: liuyuancc@gdut.edu.cn (Y.L.); xinxin.sheng@gdut.edu.cn (X.S.)
† These authors contributed equally to this work.

Abstract: In this study, ZnAl-layered double hydroxide (ZnAl-LDH) was functionalized with 2-phenylbenzimidazole-5-sulfonic acid (PBSA) to prepare ZnAl-PBSA-LDH using a simple one-step method. The electrochemical impedance spectroscopy (EIS) result of the solution phase demonstrated excellent corrosion inhibition performance of ZnAl-PBSA-LDH. Subsequently, 0.6 wt.% ZnAl-PBSA-LDH with shielding effects and active inhibition was incorporated into the water-based epoxy (WEP) for preparing the high-performance anti-corrosion coating (6-ZPL/WEP). The EIS test illustrated that the 6-ZPL/WEP coating maintained a high low-frequency impedance modulus ($|Z_{0.01\ Hz}|$) after 30 days of immersion, which is nearly two orders of magnitude higher compared to that of the blank coating. These results demonstrated that ZnAl-PBSA-LDH could efficiently improve the corrosion resistance of the WEP coating. Therefore, this study introduces new insights into the use of layered double hydroxides (LDHs) in the domain of anti-corrosion.

Keywords: ZnAl-layered double hydroxide; 2-phenylbenzimidazole-5-sulfonic acid; anti-corrosion; water-based epoxy

check for updates

Citation: Ding, C.; Wu, J.; Liu, Y.; Sheng, X.; Cheng, X.; Xiong, X.; Zhao, W. A Waterborne Epoxy Composite Coating with Smart Corrosion Resistance Based on 2-Phenylbenzimidazole-5-sulfonic Acid/Layered Double Hydroxide Composite. *Molecules* **2023**, *28*, 5199. https://doi.org/10.3390/molecules28135199

Academic Editor: Marinella Striccoli

Received: 19 May 2023
Revised: 30 June 2023
Accepted: 30 June 2023
Published: 4 July 2023

1. Introduction

Metal materials are widely used in diverse industrial fields, including parts support, oil pipelines, and ships. However, metal corrosion reduces the reliability of the metal, resulting in significant economic losses. Epoxy resin coatings have been widely employed as a preventive measure against metal corrosion due to their good adhesion, weather resistance, and chemical resistance [1]. However, traditional solvent-based epoxy resins release a volume of volatile organic compounds (VOCs) during the curing process, leading to pollution [2]. Therefore, environmentally friendly water-based epoxy (WEP) has gained attention as an anti-corrosion coating. Nevertheless, micropores and defects would be generated in the WEP coating during curing, leading to poor anti-corrosion performance. To address this issue, nanomaterials are introduced to enhance anti-corrosion performance [3–7].

Layered double hydroxides (LDHs) are a kind of layered substance made up of metal hydroxide layers with a positive charge and interlayer anions that fill the negative charges between the layers. LDHs have been widely utilized in the anti-corrosion field due to their wide surface expanse, adjustable surface chemistry, and effective ion exchange capacity [8–14]. Su et al. successfully inserted NO_2^- into the interlayer of LDHs (LDH-NO_2^-) and introduced it into resin coatings. Electrochemical testing showed that the composite coating containing LDH-NO_2^- exhibited excellent anticorrosion properties,

resulting from the shielding properties and active inhibition of corrosion of LDH-NO_2^- [15]. Buchheit et al. inserted decavanadate anions into LDH carriers and found that the VO_x^- inhibitors significantly delayed the diffusion of chloride ions on the surface of aluminum alloys [16]. Results indicate that the LDH carriers could deliver the inhibitor effectively and sustain its release for improved long-term corrosion protection. These studies demonstrated the potential of LDHs loaded with corrosion inhibitors in corrosion protection applications. However, traditional corrosion inhibitors (phosphates, chromates, and dichromates) have significant impacts on the environment and human health [17]. As a result, there is a growing need to develop green and efficient corrosion inhibitors.

2-phenylbenzimidazole-5-sulfonic acid (PBSA) is applied to absorb UVB wavelengths in sunscreen due to its ability to absorb UVB, low toxicity, and relatively easy degradation [18–20]. PBSA possesses heteroatoms (N, S) that can combine with metal ions to form complexes to inhibit corrosion, enabling its application as a candidate for green corrosion inhibitors [18,21,22]. However, previous studies have not yet investigated the application of PBSA in the domain of corrosion protection.

Hence, ZnAl-PBSA-LDH was obtained by a single-step process, wherein ZnAl-LDH was simultaneously modified during the preparation of ZnAl-LDH using zinc chloride and aluminum chloride. The successful synthesis of ZnAl-PBSA-LDH was confirmed through chemical and physical characterization techniques. Additionally, EIS was employed to analyze the corrosion inhibition properties of ZnAl-PBSA-LDH in a 3.5 wt.% solution. Subsequently, ZnAl-PBSA-LDH was incorporated into WEP coatings to enhance their corrosion resistance. Lastly, the potential synergistic effect between PBSA and LDHs in improving the protective properties of the coatings was explored.

2. Results and Discussion

2.1. Characterization of MgAl-CO_3^{2-}-LDH, ZnAl-NO_3^--LDH, and ZnAl-PBSA-LDH

The morphology of MgAl-CO_3^{2-}-LDH, ZnAl-NO_3^--LDH, and ZnAl-PBSA-LDH was observed using SEM. Figures 1(b_1) and S1 show the microscopic morphology of ZnAl-NO_3^--LDH, which resulted from the merging together of numerous small flake-like crystals [23]. After the insertion of PBSA, the morphology of the crystals was bulky (Figure 1(c_1)). Furthermore, EDS mappings were utilized to analyze the elements distribution of the nanomaterial to confirm the success of modification. As Figure 1(c_2–c_4) shows, the presence of the Zn, Al, and S elements demonstrated the successful preparation of ZnAl-PBSA-LDH. The insertion of PBSA contributes to the improvement of the activity inhibition of LDHs.

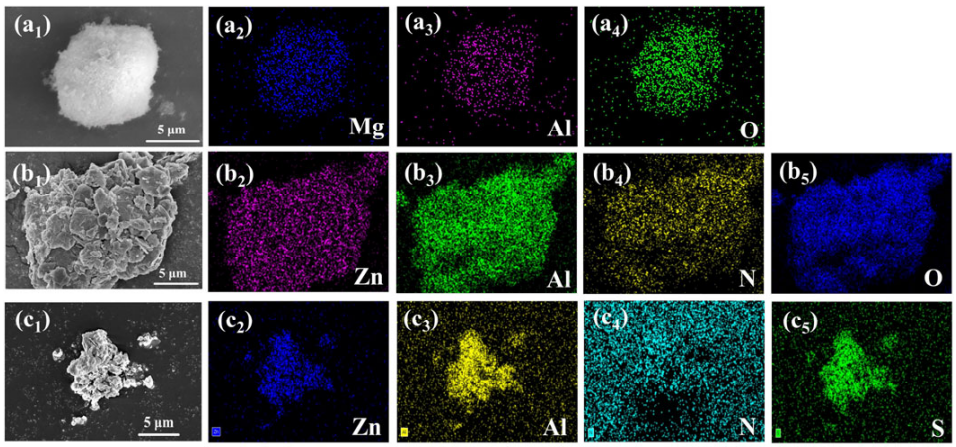

Figure 1. SEM images of (**a_1**) MgAl-CO_3^{2-}-LDH and its EDS mapping corresponds to (**a_2**) Mg, (**a_3**) Al, and (**a_4**) O, SEM images of (**b_1**) ZnAl-NO_3^--LDH and its EDS mapping corresponds to (**b_2**) Zn, (**b_3**) Al, (**b_4**) N, and (**b_5**) O. SEM images of (**c_1**) ZnAl-PBSA-LDH and its EDS mapping corresponds to (**c_2**) Zn, (**c_3**) Al, (**c_4**) N, and (**c_5**) S.

The crystal structure of the nanomaterials was investigated using X-ray diffraction (XRD). As Figure 2a shows, diffraction peaks at (003), (006), and (012) were detected in the curve of MgAl-CO_3^{2-}-LDH, demonstrating the successful synthesis of MgAl-CO_3^{2-}-LDH. Furthermore, the characteristic peaks of ZnAl-NO_3^--LDH were detected at 2θ values of 9.91°, 19.90°, and 30.04°, which were assigned to the (003), (006), and (009) peaks, respectively [24–26]. The (003) peak corresponds to a d-spacing value of 0.89 nm, consistent with previous reports [27–30]. After intercalation of PBSA, the (003) peak of ZnAl-PBSA-LDH shifted to 4.12°, indicating an increase in the d-spacing to 2.14 nm. This significant change indicates the successful intercalation of PBSA into the LDH layers.

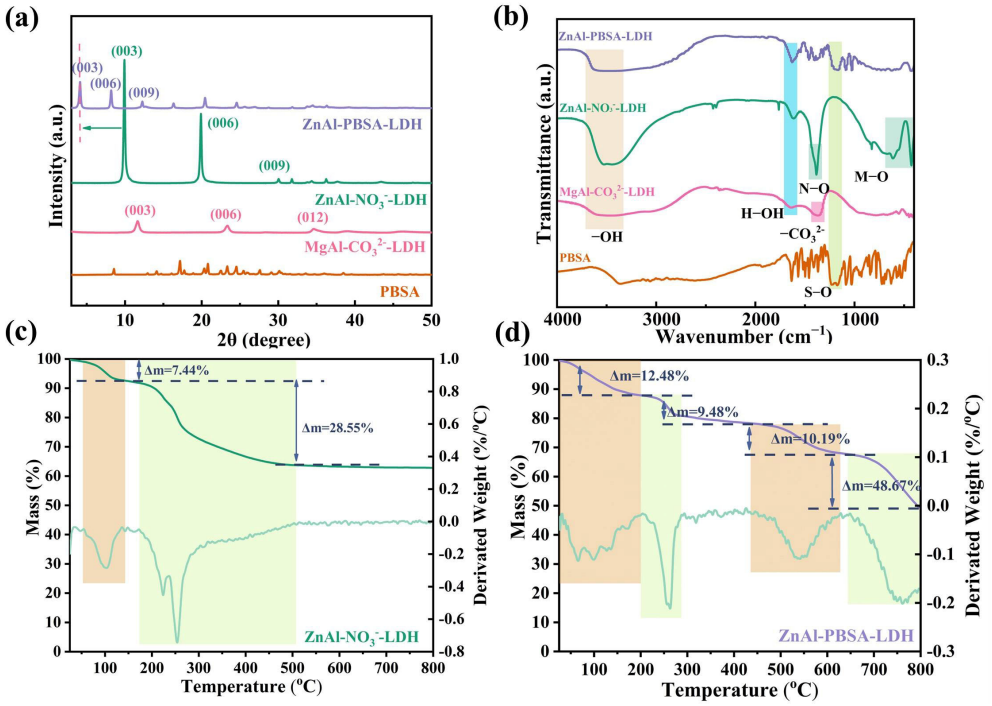

Figure 2. (**a**) XRD curves; (**b**) FTIR curves; TG-DTG curves of (**c**) ZnAl-NO_3^--LDH and (**d**) ZnAl-PBSA-LDH.

Fourier-transform infrared spectroscopy (FTIR) was used to analyze the chemical composition of ZnAl-NO_3^--LDH, ZnAl-PBSA-LDH, MgAl-CO_3^{2-}-LDH, and PBSA. In Figure 2b, the peaks observed at 3463 cm^{-1} and 1628 cm^{-1} in the FTIR curve of ZnAl-NO_3^--LDH correspond to the stretching vibration of the −OH bond and the deformation vibration of water molecules, respectively [18,24–32]. Additionally, the N−O peak at 1387 cm^{-1} provided evidence for the successful intercalation of NO_3^- ions into the LDH layers. Moreover, the stretching and bending modes of metal-oxygen (Zn−O and Al−O) are observed at a sequence of absorption bands that occur below 1000 cm^{-1} [33,34]. Collectively, these findings confirm the successful synthesis of ZnAl-NO_3^--LDH. In comparison to ZnAl-NO_3^--LDH, the FTIR spectrum of ZnAl-PBSA-LDH revealed a novel peak at 1183 cm^{-1}. This peak corresponded to the S−O bond vibration from PBSA, indicating the successful intercalation of PBSA into the LDH layers.

Thermogravimetric analysis (TGA) can provide effective information for the intercalation of PBAS into LDH layers. As shown in Figure S2, the TG-DTG curve of PBSA displayed two weight-loss stages due to the thermal breakdown of water molecules and PBSA. In Figure 2c, ZnAl-NO_3^--LDH showed two main weight-loss stages, corresponding to the thermal decomposition of water molecules and nitrates, respectively [35]. As shown in Figure 2d, ZnAl-PBSA-LDH exhibited four main weight-loss stages. The initial phase of weight loss was attributed to the loss of water molecules and a small amount of nitrate. The second weight loss stage of ZnAl-PBSA-LDH from 200 to 287 °C was associated with

the loss of nitrates. The last two weight-loss stages were attributed to the thermal decomposition of PBSA. These results demonstrated that PBSA was successfully inserted into the interlayer of LDHs.

2.2. Characterization of Nanocomposite Coatings

In order to evaluate the compatibility of fillers with coatings, SEM and EDS mappings were used to observe the fracture surface of coatings. For the blank coating, deep holes were present on the smooth fracture surface (yellow circle in Figure 3b). The corrosive ions could easily corrode the steel through these pores. In contrast, the 6-ZPL/WEP coating without holes exhibited homogeneous cracks (Figure 3e), demonstrating the excellent compatibility of ZnAl-PBSA-LDH and WEP coatings, which is beneficial for the improvement of the barrier properties of coatings. However, some agglomerations of ZnAl-PBSA-LDH were observed in the fracture surface of the 8-ZPL/WEP coating (yellow circle in Figure 3h), suggesting the poor dispersion of excessive ZnAl-PBSA-LDH within the WEP coating. Additionally, EDS mapping of the 6-ZPL/WEP coating (Figure 3i) indicated that 0.6 wt.% ZnAl-PBSA-LDH was uniformly distributed across the WEP matrix. The excellent compatibility and dispersion of ZnAl-PBSA-LDH in the WEP coating are conducive to reducing the porosity of the WEP coating, resulting in the improvement of anti-corrosion properties.

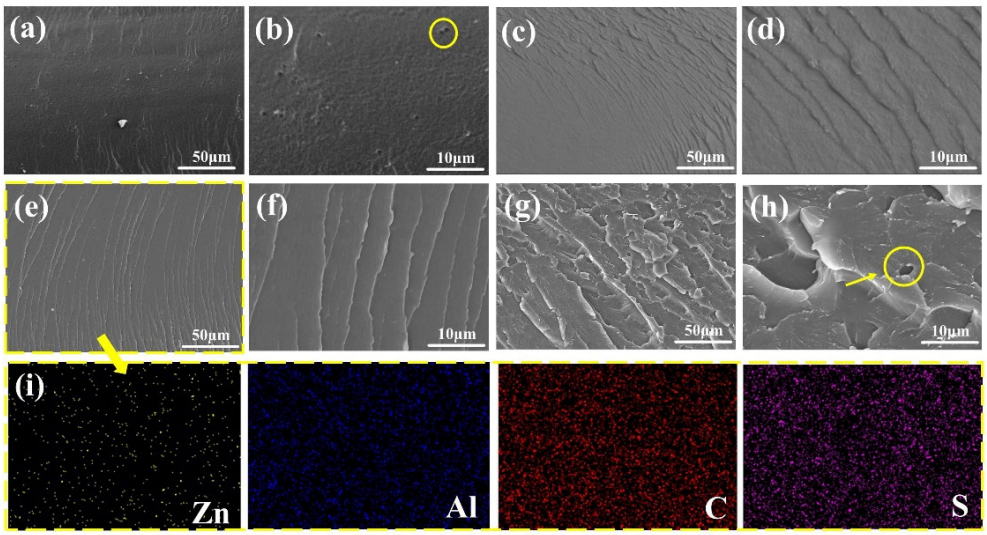

Figure 3. SEM images of the fractured surface of (**a**,**b**) blank WEP, (**c**,**d**) 4-ZPL/WEP, (**e**,**f**) 6-ZPL/WEP, and (**g**,**h**) 8-ZPL/WEP. The EDS mapping of (**i**) 6-ZPL/WEP.

2.3. Electrochemical Measurements

EIS of the solution phase was utilized to explore the corrosion inhibition of LDHs and further select inhibitors that could subsequently be employed to enhance the corrosion resistance of WEP coatings. The corrosion inhibition of the inhibitors was evaluated using low-frequency impedance modulus ($|Z_{0.01\ Hz}|$) [36]. During the initial stages of immersion (1 h), the ZnAl-NO_3^--LDH sample exhibited the highest $|Z_{0.01\ Hz}|$ value among all samples (Figure 4b). However, after 72 h, the $|Z_{0.01\ Hz}|$ value of ZnAl-NO_3^--LDH significantly decreased (Figure 4h), indicating its limited corrosion inhibition capacity. For MgAl-CO_3^{2-}-LDH, the $|Z_{0.01\ Hz}|$ value was lower than that of ZnAl-NO_3^--LDH during the corrosion process, implying that MgAl-CO_3^{2-}-LDH exhibited worse corrosion inhibition for Q215 steel. In contrast, the ZnAl-PBSA-LDH sample exhibited the highest impedance modulus among all the samples after 72 h (Figure 4h), demonstrating the excellent corrosion inhibition ability of ZnAl-PBSA-LDH.

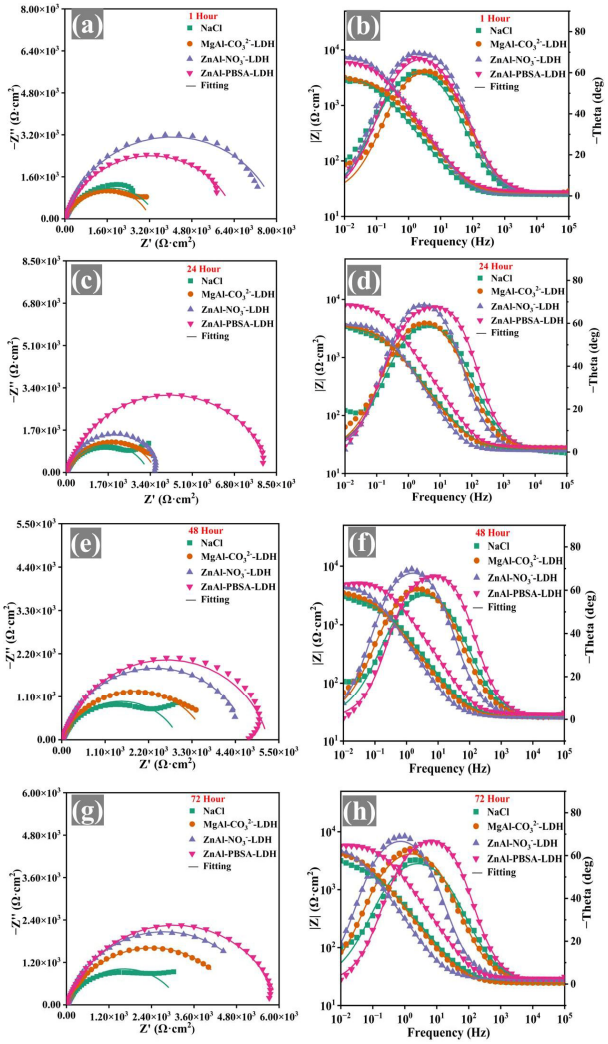

Figure 4. Nyquist plots and Bode-phase plots of the immersed bare steel samples in the blank solution and the extracted solutions of NaCl, MgAl-CO_3^{2-}-LDH, ZnAl-NO_3^{-}-LDH, and ZnAl-PBSA-LDH for (**a**,**b**) 1 h, (**c**,**d**) 24 h, (**e**,**f**) 48 h, and (**g**,**h**) 72 h.

The EIS results were fitted with an equivalent circuit by ZSimpwin software and are shown in Table S1 [37]. R_s represents the solution resistance. CPE_f and R_f correspond to film capacitance and resistance. Additionally, CPE_{dl} (double-layer capacitance) and R_{ct} (charge transfer resistance) reflect the underlying interfacial mechanisms. The CPE_{dl} values of steel immersed in ZnAl-PBSA-LDH extract were lower than that of other samples, implying that ZnAl-PBSA-LDH exhibited good corrosion inhibition [38]. To further explore the corrosion inhibition of corrosion inhibitors, the capacitance corresponding to the film and double-layer capacitors was calculated using Equations (1) and (2) [39]. The results are listed in Table S1.

$$C_f = Y_{0,f}^{\frac{1}{n}} \times R_f^{\frac{(1-n)}{n}} \quad (1)$$

$$C_{dl} = Y_{0,dl}^{\frac{1}{n}} \times \left(\frac{R_s \times R_{ct}}{R_s + R_{ct}} \right)^{\frac{(1-n)}{n}} \quad (2)$$

The C_f values were applied to evaluate the barrier performance of a protective film composed of inhibitors and iron ions [36]. During the initial stage of steel immersion in the extracted solution of ZnAl-PBSA-LDH (Table S1), the C_f value of the ZnAl-PBSA-LDH sample was found to be the highest compared to the other periods (24 h, 48 h, and 72 h), indicating insufficient barrier performance of the film composed of PBSA and Fe

ions. Moreover, the C_f values showed a decreasing trend as the immersion time increased, illustrating that the film progressively became denser and thicker. It is because PBSA with heteroatoms (N, S) combined with metal ions and formed complexes [40]. Additionally, the samples with lower C_{dl} values display a higher inhibition effect [36]. The C_{dl} values of ZnAl-PBSA-LDH were the lowest compared to other samples, demonstrating the excellent activity inhibition of ZnAl-PBSA-LDH. Therefore, ZnAl-PBSA-LDH was utilized to improve the anti-corrosion properties of the WEP coating.

EIS testing was conducted to assess the corrosion resistance of coated samples. The large diameter of the capacitor arc in the Nyquist plots indicates that the coatings provided good corrosion protection [41]. As shown in Figure 5, the capacitance arc diameter of composite coatings containing the ZnAl-PBSA-LDH was larger than that of blank coating, indicating that ZnAl-PBSA-LDH could effectively improve the corrosion resistance of the WEP coating. In addition, at a low frequency, the resistive component dominates the impedance of a coating. Hence, the $|Z_{0.01\ Hz}|$ value is utilized to evaluate the barrier properties of the coatings [42]. In Figure 6, the composite coatings containing ZnAl-PBSA-LDH exhibited a higher $|Z_{0.01\ Hz}|$ than that of a blank WEP coating after 30 days of immersion, demonstrating that ZnAl-PBSA-LDH can effectively improve the barrier performance of the coating. However, the 8-ZPL/WEP coating exhibited a lower $|Z_{0.01\ Hz}|$ than that of 0.6 ZnAl-PBSA/WEP coating, which is caused by the aggregation of ZnAl-PBSA-LDH in the WEP coating. The breakpoint frequency (f_b) was utilized to assess the layered area of the WEP coating and steel [43]. As shown in Figure S3c, the f_b value of blank WEP coating increased to 204.6 Hz after soaking for 30 days, implying that blank coating has difficulty effectively protecting the substrate. In contrast, 6-ZPL/WEP coating exhibited a low f_b value (0.45 Hz), indicating that ZnAl-PBSA-LDH significantly enhanced the corrosion resistance of coatings. On the one hand, ZnAl-PBSA-LDH can inhibit the diffusion of corrosive ions via the shielding effect; on the other hand, the released PBSA can form a complex film with iron ions that protect the steel.

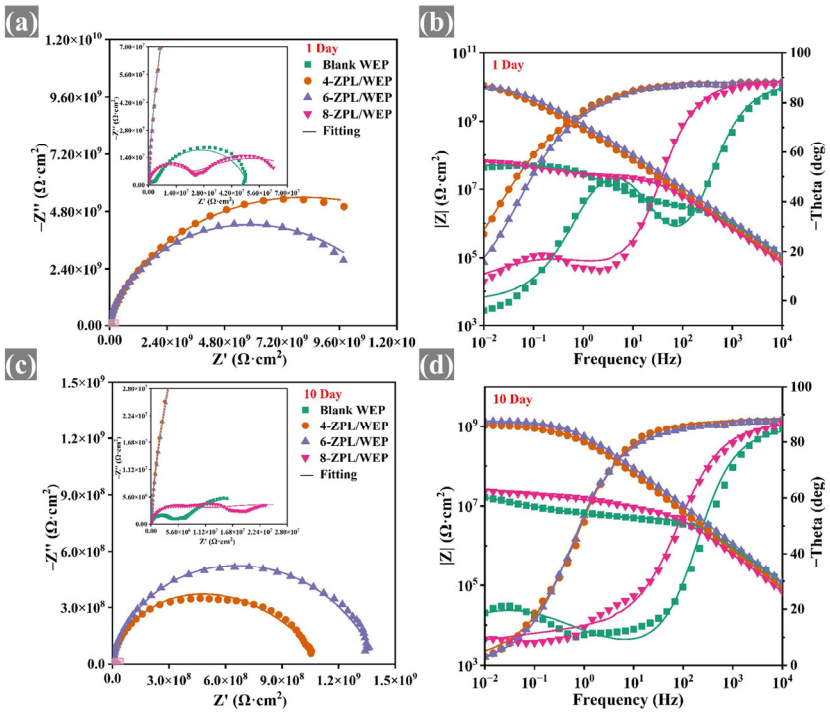

Figure 5. (**a**,**c**) Nyquist and (**b**,**d**) Bode plots of coated samples after 10 days immersion.

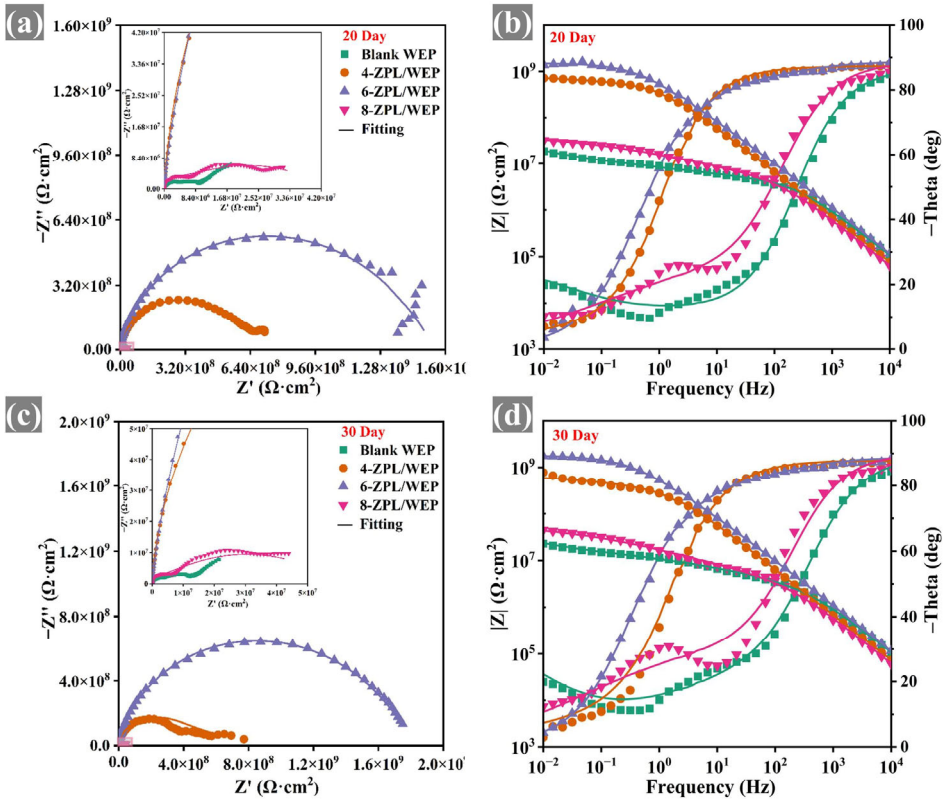

Figure 6. (**a**,**c**) Nyquist and (**b**,**d**) Bode plots of coated samples after 30 days immersion.

The equivalent electrical circuit (EEC) models shown in Figure S3d were employed to analyze the EIS results. The parameters R_f and R_{ct} represent the resistance of the coating and the charge transfer resistance, respectively. In addition, CPE_c and CPE_{dl} correspond to the non-constant phase capacitance and double-layer capacitance of the coating, respectively. R_f was applied to evaluate the porosity of the coatings [44]. Figure S3a and Table S2 demonstrate that the blank WEP coating exhibited a low R_f value (1.5×10^6 Ω·cm^2) after 30 days, indicating that the blank WEP coating was ineffective in providing sufficient protection to the substrate. In contrast, the 6-ZPL/WEP coating exhibited a high R_f value of 2.52×10^7 Ω·cm^2, which was 16.8 times that of the blank WEP coating. This suggests that ZnAl-PBSA-LDH can effectively reduce the porosity of the coating and enhance its corrosion resistance. Nevertheless, the R_f value of the 8-ZPL/WEP coating (1.9×10^6 Ω·cm^2) was lower than that of the 6-ZPL/WEP coating after 30 days of immersion, which was attributed to the agglomeration of excessive ZnAl-PBSA-LDH within the WEP coating. In summary, the 6-ZPL/WEP coating had the highest R_f and largest capacitance arc diameter among all coatings after 30 days of immersion, illustrating its excellent corrosion resistance.

After subjecting the coated samples to a 30-day of immersion, potentiodynamic polarization (PD) testing was employed to further explore the corrosion resistance of the coating. The related results are shown in Figure 7. Subsequently, the corresponding electrochemical parameters were calculated and listed in Table 1, such as corrosion rate (CR), polarization resistance (R_p), current density (I_{corr}), corrosion potential (E_{corr}), anode (b_a), and cathode (b_c). E_{corr} was utilized to evaluate the possibility of corrosion. In Figure 7, the 6-ZPL/WEP coating exhibited the most positive E_{corr} among all the coatings, implying a lower probability of corrosion for steel coated with the 6-ZPL/WEP coating. In addition, I_{corr} is an important index to use to measure the corrosion resistance of coatings. Generally, a lower I_{corr} value indicates better corrosion protection provided by the coating [44]. As shown in Table 1, the 6-ZPL/WEP coating exhibited the lowest I_{corr} value among all the samples, suggesting excellent corrosion performance. The excellent corrosion resistance of the 6-ZPL/WEP coating can be attributed to multiple contributing factors. Firstly, the ZnAl-

PBSA-LDH nanomaterials can effectively prevent the diffusion of the corrosion medium via the shielding effect [45]. Secondly, the favorable compatibility between ZnAl-PBSA-LDH and WEP is beneficial for the construction of the "maze effect", thereby prolonging the diffusion path of corrosive ions [34]. Thirdly, the released PBSA can be complexed with metal ions to establish a film that can inhibit corrosion; Lastly, LDHs with unique layered structures could attract chloride ions and prevent Cl^- from interacting with the metal surface, causing corrosion inhibition [46].

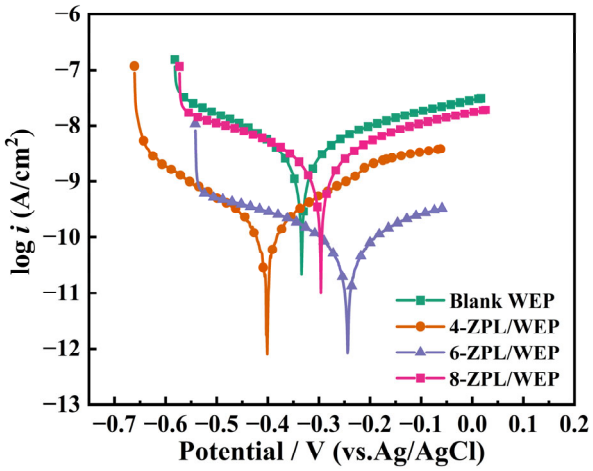

Figure 7. Potentiodynamic polarization curves of all coatings after 30 days of immersion in 3.5 wt.% NaCl solution.

Table 1. Tafel extrapolation results obtained from Figure 7.

Sample	E_{corr} (mV)	I_{corr} (A/cm^2)	R_p (Ω·cm^2)	b_a (mV/dec)	b_c (mV/dec)	CR (mpy)
Blank WEP	−3340	3.225×10^{-9}	1.29×10^{7}	209.12	−176.55	4.72×10^{-4}
4-ZPL/WEP	−4010	1.986×10^{-10}	1.93×10^{8}	175.60	−177.56	2.90×10^{-5}
6-ZPL/WEP	−2440	8.012×10^{-11}	5.49×10^{8}	205.55	−198.93	1.17×10^{-5}
8-ZPL/WEP	−2960	2.286×10^{-9}	1.91×10^{7}	199.40	−203.42	3.34×10^{-4}

SEM and EDS were applied to evaluate the degree of corrosion of the substrate after 30 days of immersion. Figure 8a depicts the substantial amount of rust that appeared on the surface of the steel protected by the blank WEP coating, illustrating the poor corrosion protection provided by the blank WEP coating. In contrast, a small loose rust layer appeared on the surface of the substrate coated with the 4-ZPL/WEP coating (Figure 8b), implying that ZnAl-PBSA-LDH with its shielding effect and activity inhibition can effectively improve the anti-corrosion properties of WEP. For the steel coated with the 6-ZPL/WEP coating, there were no noticeable signs of corrosion, indicating that the 6-ZPL/WEP coating exhibited excellent protection. Furthermore, EDS was utilized to measure the oxygen content of the substrate surface to assess the degree of corrosion [47]. Figure 8(c_1) showed that the surface of the steel coated with the 6-ZPL/WEP coating exhibited a low oxygen content (7.1%), which was decreased by 84.6% compared to that of the blank WEP coating (46%), indicating that the 6-ZPL/WEP coating provides excellent protection for the substrate. Chloride ions play a major role in the corrosion process as they can adsorb onto the metal surface, causing damage to the metal surface [48]. As shown in Figure 8, the chloride ion content of the composite coatings was lower than that of the blank WEP coating, which is caused by the unique layered structure of LDHs. LDHs can selectively adsorb and immobilize chloride ions via electrostatic interactions, further hindering the diffusion of chloride ions and protecting the steel.

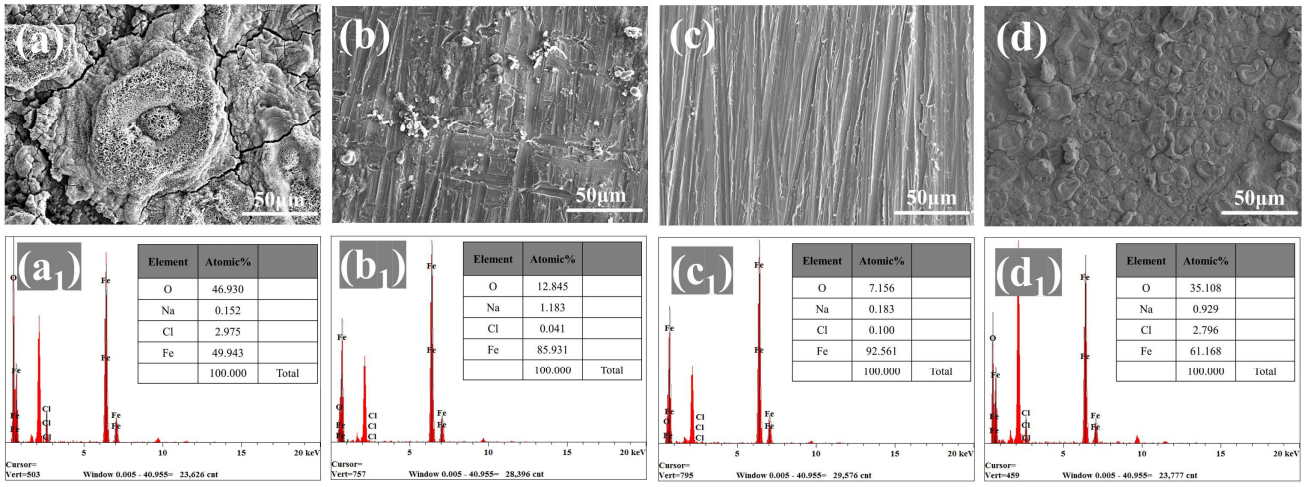

Figure 8. SEM images and EDS mapping of substrates coated by (**a**,**a**$_1$) blank WEP, (**b**,**b**$_1$) 4-ZPL/WEP, (**c**,**c**$_1$) 6-ZPL/WEP, and (**d**,**d**$_1$) 8-ZPL/WEP coatings after immersion of 30 days.

As shown in Figure 9a, corrosive media such as H_2O and Cl^- can easily spread to steel surfaces from the micropores and microcracks of the blank WEP coating, resulting in corrosion. In contrast, ZnAl-PBSA-LDH nanomaterials may effectively stop the spread of the corrosion medium through the shielding effect. Simultaneously, the released PBSA could combine with the metal ion and adsorb on the surface of the substrate, resulting in a complex film that protects the substrate from corrosion. Additionally, ZnAl-PBSA-LDH captures Cl^- in solution, thereby reducing the interaction between Cl^- and steel [24]. In summary, ZnAl-PBSA-LDH, with its shielding effects and activity inhibition, can effectively improve the anticorrosion properties of the coating.

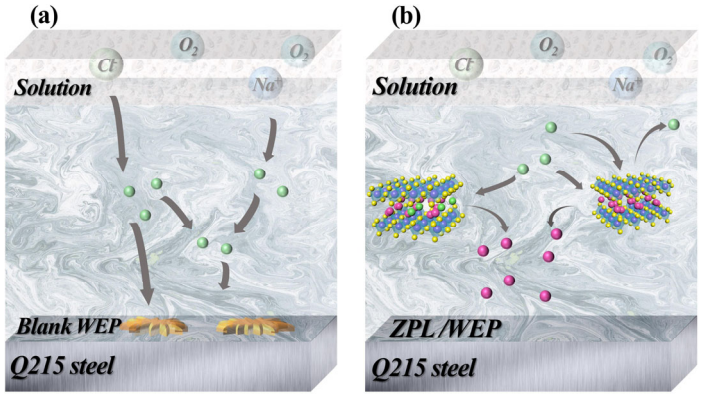

Figure 9. Anti-corrosion mechanism of (**a**) blank WEP and (**b**) ZPL/WEP.

3. Materials and Methods

3.1. Materials

Zinc chloride ($ZnCl_2$), aluminum chloride hexahydrate ($AlCl_3{\cdot}6H_2O$), magnesium chloride hexahydrate ($MgCl_2{\cdot}6H_2O$), sodium carbonate (Na_2CO_3), sodium nitrate ($NaNO_3$), and sodium hydroxide (NaOH) were purchased from Macklin Biochemical Co., Ltd. (Shanghai, China) PBSA was purchased from Yuanye Bio-Technology Co., Ltd. (Shanghai, China). The Q215 steel used in the study was purchased from Oudifu Co., Ltd. The elemental content (wt.%) of Q215 steel (abbreviated Q215) was found to be: C $\leq$ 0.15; S $\leq$ 0.05; P $\leq$ 0.05; Si $\leq$ 0.35; Mn $\leq$ 1.20; and balance Fe. E51 (epoxide equivalent weight = 196) was obtained from Dongfeng Chemicals Co., Ltd., Guangzhou, China. The curing agent used was BANCO901, which has an active hydrogen equivalent value of 248, supplied by B & C Chemicals Co., Ltd. (Shanghai, China).

3.2. Preparation of MgAl-CO_3^{2-}-LDH

The MgAl-CO_3^{2-}-LDH was synthesized using the conventional coprecipitation method. Initially, a mixture of 0.5 M $MgCl_2 \cdot 6H_2O$ and 0.25 M $AlCl_3 \cdot 6H_2O$ (V = 50 mL) was slowly added dropwise into a solution of 0.25 M Na_2CO_3 (V = 100 mL) while adjusting the pH to 9 ± 0.5 with sodium hydroxide, then stirring for 2 h at 35 °C. The resulting white precipitate was then crystallized at 70 °C for 24 h. Subsequently, the mixture solution was filtered to remove all supernatants, and the sample was washed several times with distilled water. Finally, the sample was dried in a vacuum oven at 80 °C.

3.3. Preparation of ZnAl-NO_3^--LDH

The preparation of *ZnAl-NO_3^--LDH* needs to be completed under a nitrogen atmosphere. Initially, a mixture of 0.5 M $ZnCl_2 \cdot 6H_2O$ and 0.25 M $AlCl_3 \cdot 6H_2O$ (V = 50 mL) was slowly added dropwise into a solution of 0.25 M $NaNO_3$ (V = 100 mL) while adjusting the pH to 9 ± 0.5 with sodium hydroxide and stirring for 2 h at 35 °C. Then, the resulting mixture solution was left at 70 °C for 24 h. Subsequently, the mixture solution was filtered to remove all supernatants, and the sample was washed several times with distilled water. Finally, the sample was dried in a vacuum oven at 80 °C to obtain ZnAl-NO_3^--LDH.

3.4. Preparation of ZnAl-LDHs Loaded with PBSA

The preparation of *ZnAl-PBSA-LDH* needs to be completed under a nitrogen atmosphere. First, the determined amounts of $ZnCl_2$ solution and $AlCl_3 \cdot 6H_2O$ solution were added slowly to the flask via a constant pressure drip funnel under vigorous stirring at a temperature of 35 °C. Subsequently, 100 mL of PBSA solution was slowly dropped into the mixed solution. Then, sodium hydroxide was used to adjust the pH of the solution to 9. The mixed solution was stirred for 2 h, following which the white precipitate was subjected to aging at a temperature of 70 °C for 24 h. Subsequently, the mixture was filtered to remove all the supernatant. The resulting sample was washed several times using degassed distilled water and then dried at 80 °C in a vacuum oven.

3.5. Coating Preparation

The Q215 substrate, measuring 120 mm × 120 mm × 1 mm, underwent a preparation process before the application of the composite coating. Initially, the substrate was polished using sandpaper ranging from 180 to 600 grades. Subsequently, the substrate was degreased using ethanol. The composite coating was made by mixing BANCO901, E51, deionized water, and fillers (ZnAl-PBSA-LDH of 0.4 wt.%, 0.6 wt.%, 0.8 wt.%) using sonication for 10 min. The composite coatings were applied to the pre-treated Q215 substrate by a four-sided applicator with a wet thickness of 100 μm. After drying at room temperature for 7 days, the coating was further dried at 75 °C for 6 h. The final thickness of the dried coating was 40 ± 2 μm. The experimental flow chart is shown in Figure 10.

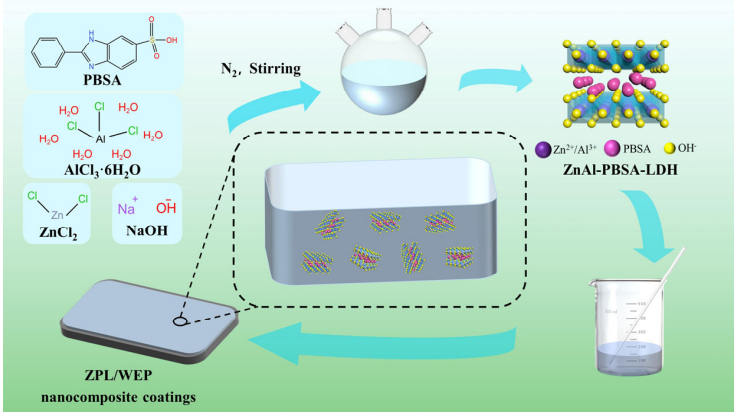

Figure 10. Schematic diagram of the synthesis and preparation of the LDH coating.

3.6. Characterization

Fourier transform infrared (FTIR) analysis was performed using the Thermo Fisher Scientific Nicolet iS50R Spectrometer (Waltham, MA, USA). The phase composition was analyzed by X-ray diffraction (XRD) using the Rigaku MiniFlex600, which uses Cu-Kα radiation (λ = 0.15406 nm) in a scanning range of 2θ = 3° to 70° at a rate of 10°/min. Furthermore, the thermal stability of the samples was investigated by thermogravimetric (TG) using the Netzsch STA449F5 Jupiter, in the N2 atmosphere with a temperature range of 25–800 °C and a heating rate of 10 °C/min. The microstructure and morphology of fillers were characterized by field emission scanning electron microscopy (FESEM, Apreo 2S HiVac, Waltham, MA, USA). Moreover, the fracture surface of the coatings was studied using energy dispersive spectroscopy (EDS, Bruker XFlash, Billerica, MA, USA) in combination with SEM (JEOL S-3400N, Tokyo, Japan).

3.7. Electrochemical Measures

The electrochemical impedance spectroscopy (EIS) test was conducted to evaluate the effect of the extract on bare metal corrosion in NaCl (3.5 wt.%) solution. The concentration of the inhibitors in the extracted solutions is all 0.4 wt.%. Furthermore, EIS and potentiodynamic polarization (PD) tests were utilized to evaluate the anticorrosion properties of the coating in 3.5 wt.% NaCl. The EIS and PD tests were performed using the CHI760E electrochemical workstation and a device consisting of Ag/AgCl, graphite, and steel with an exposed area of 3.14 cm^2. The EIS and PD tests were conducted using a stable open-circuit potential and an amplitude of 10 mV across a frequency range of 10^5–10^{-2} Hz. After 30 days of immersion, the corrosion products of the intact coated samples were observed using SEM.

4. Conclusions

This study successfully synthesized ZnAl-PBSA-LDH materials using a simple one-step approach. The successful preparation of ZnAl-PBSA-LDH was confirmed by SEM, XRD, and FTIR. Then, different amounts of ZnAl-PBSA-LDH were incorporated into the WEP coating to prepare a high-performance anti-corrosion coating. The SEM and EDS results showed that ZnAl-PBSA-LDH exhibited good dispersibility with the WEP coating. The results of electrochemical measures showed that the 6-ZPL/WEP coating exhibited a high $|Z_{0.01\,Hz}|$ value ($10^{9.24}$ Ω·cm^2), which was almost two orders of magnitude higher than that of the blank WEP coating. This indicates that ZnAl-PBSA-LDH could effectively improve the corrosion resistance of the coating due to its shielding effect, activity inhibition, and ion exchange. Overall, we have successfully used this feature to produce lightweight, high-performance WEP composite coatings, highlighting the significant potential of LDHs in the field of anti-corrosion.

Supplementary Materials: The following supporting information can be downloaded at: https://www.mdpi.com/article/10.3390/molecules28135199/s1, Figure S1: SEM images of ZnAl-NO_3^--LDH. Figure S2: TG-DTG curves of (a) MgAl-CO_3^{2-}-LDH and (b) PBSA. Figure S3: The changes of (a) Rf values, (b) $|Z_{0.01\,Hz}|$ values, (c) fb values; (d) the equivalent electrical circuits. Table S1: The parameters obtained from the fitting of EIS data are related to the uncoated samples exposed to the blank and inhibited solutions. Table S2: The parameters obtained from the fitting of EIS data related to the coated samples immersed in 3.5 wt.% NaCl solution.

Author Contributions: Methodology, validation, data curation, writing—original draft, C.D.; investigation, writing—review & editing, data curation, J.W.; supervision, project administration, resources, funding acquisition, Y.L.; writing—review & editing, supervision, project administration, X.S.; resources, project administration, X.C.; resources, supervision, X.X.; resources, funding acquisition, W.Z. All authors have read and agreed to the published version of the manuscript.

Funding: This work was supported by the Research Funding of GCH Technology Co., Ltd. (No. 607210383), and the authors also acknowledge the support from Demonstration Base for Joint Training of Postgraduates between Guangdong University of Technology and GCH Technology Co., Ltd.

Institutional Review Board Statement: Not applicable.

Informed Consent Statement: Not applicable.

Data Availability Statement: Data of the present study are available in the article.

Conflicts of Interest: The authors declare no conflict of interest.

Sample Availability: Samples of the compounds are available from the authors.

References

1. Liu, B.; Wang, Y. A Novel Design for Water-Based Modified Epoxy Coating with Anti-Corrosive Application Properties. *Prog. Org. Coat.* **2014**, *77*, 219–224. [CrossRef]
2. Wu, J.; Chen, Y.; Zhang, L.; Sheng, X. Construction of a High-Performance Anti-Corrosion and Anti-Wear Coating Based on the MXene@PTA-Zn(II): Electrochemical/Tribological Investigations. *Prog. Org. Coat.* **2023**, *182*, 107706. [CrossRef]
3. Tian, H.; Li, W.; Liu, A.; Gao, X.; Han, P.; Ding, R.; Yang, C.; Wang, D. Controlled Delivery of Multi-Substituted Triazole by Metal-Organic Framework for Efficient Inhibition of Mild Steel Corrosion in Neutral Chloride Solution. *Corros. Sci.* **2018**, *131*, 1–16. [CrossRef]
4. Zhang, Z.; Zhang, W.; Li, D.; Sun, Y.; Wang, Z.; Hou, C.; Chen, L.; Cao, Y.; Liu, Y. Mechanical and Anticorrosive Properties of Graphene/Epoxy Resin Composites Coating Prepared by in-Situ Method. *Int. J. Mol. Sci.* **2015**, *16*, 2239–2251. [CrossRef]
5. Hayatgheib, Y.; Ramezanzadeh, B.; Kardar, P.; Mahdavian, M. A Comparative Study on Fabrication of a Highly Effective Corrosion Protective System Based on Graphene Oxide-Polyaniline Nanofibers/Epoxy Composite. *Corros. Sci.* **2018**, *133*, 358–373. [CrossRef]
6. Cui, M.; Ren, S.; Chen, J.; Liu, S.; Zhang, G.; Zhao, H.; Wang, L.; Xue, Q. Anticorrosive Performance of Waterborne Epoxy Coatings Containing Water-Dispersible Hexagonal Boron Nitride (h-BN) Nanosheets. *Appl. Surf. Sci.* **2017**, *397*, 77–86. [CrossRef]
7. Huang, H.; Li, M.; Tian, Y.; Xie, Y.; Sheng, X.; Jiang, X.; Zhang, X. Exfoliation and Functionalization of α-Zirconium Phosphate in One Pot for Waterborne Epoxy Coatings with Enhanced Anticorrosion Performance. *Prog. Org. Coat.* **2020**, *138*, 105390. [CrossRef]
8. Sjåstad, A.O.; Andersen, N.H.; Vajeeston, P.; Karthikeyan, J.; Arstad, B.; Karlsson, A.; Fjellvåg, H. On the Thermal Stability and Structures of Layered Double Hydroxides $Mg_{1-X}Al_x(OH)_2(NO_3)_X{\cdot}mH_2O$ ($0.18 \leq x \leq 0.38$). *Eur. J. Inorg. Chem.* **2015**, *2015*, 1775–1788. [CrossRef]
9. Nguyen Thuy, D.; To Thi Xuan, H.; Nicolay, A.; Paint, Y.; Olivier, M.-G. Corrosion Protection of Carbon Steel by Solvent Free Epoxy Coating Containing Hydrotalcites Intercalated with Different Organic Corrosion Inhibitors. *Prog. Org. Coat.* **2016**, *101*, 331–341. [CrossRef]
10. Neves, C.S.; Bastos, A.C.; Salak, A.N.; Starykevich, M.; Rocha, D.; Zheludkevich, M.L.; Cunha, A.; Almeida, A.; Tedim, J.; Ferreira, M.G.S. Layered Double Hydroxide Clusters as Precursors of Novel Multifunctional Layers: A Bottom-Up Approach. *Coatings* **2019**, *9*, 328. [CrossRef]
11. Zhang, F.; Zhang, C.; Song, L.; Zeng, R.; Liu, Z.; Cui, H. Corrosion of In-Situ Grown MgAl-LDH Coating on Aluminum Alloy. *Trans. Nonferrous Met. Soc. China* **2015**, *25*, 3498–3504. [CrossRef]
12. Zhang, F.; Liu, Z.-G.; Zeng, R.-C.; Li, S.-Q.; Cui, H.-Z.; Song, L.; Han, E.-H. Corrosion Resistance of Mg–Al-LDH Coating on Magnesium Alloy AZ31. *Surf. Coat. Technol.* **2014**, *258*, 1152–1158. [CrossRef]
13. Zubair, M.; Daud, M.; McKay, G.; Shehzad, F.; Al-Harthi, M.A. Recent Progress in Layered Double Hydroxides (LDH)-Containing Hybrids as Adsorbents for Water Remediation. *Appl. Clay Sci.* **2017**, *143*, 279–292. [CrossRef]
14. Zhao, M.; Zhao, Q.; Li, B.; Xue, H.; Pang, H.; Chen, C. Recent Progress in Layered Double Hydroxide Based Materials for Electrochemical Capacitors: Design, Synthesis and Performance. *Nanoscale* **2017**, *9*, 15206–15225. [CrossRef] [PubMed]
15. Su, Y.; Qiu, S.; Yang, D.; Liu, S.; Zhao, H.; Wang, L.; Xue, Q. Active Anti-Corrosion of Epoxy Coating by Nitrite Ions Intercalated MgAl LDH. *J. Hazard. Mater.* **2020**, *391*, 122215. [CrossRef] [PubMed]
16. Buchheit, R.G.; Guan, H.; Mahajanam, S.; Wong, F. Active Corrosion Protection and Corrosion Sensing in Chromate-Free Organic Coatings. *Prog. Org. Coat.* **2003**, *47*, 174–182. [CrossRef]
17. Salleh, S.Z.; Yusoff, A.H.; Zakaria, S.K.; Taib, M.A.A.; Abu Seman, A.; Masri, M.N.; Mohamad, M.; Mamat, S.; Ahmad Sobri, S.; Ali, A.; et al. Plant Extracts as Green Corrosion Inhibitor for Ferrous Metal Alloys: A Review. *J. Clean. Prod.* **2021**, *304*, 127030. [CrossRef]
18. Mohsin, S.M.N.; Hussein, M.Z.; Sarijo, S.H.; Fakurazi, S.; Arulselvan, P.; Taufiq-Yap, Y.H. Nanolayered Composite with Enhanced Ultraviolet Ray Absorption Properties from Simultaneous Intercalation of Sunscreen Molecules. *Int. J. Nanomed.* **2018**, *13*, 6359. [CrossRef]
19. Ji, Y.; Zhou, L.; Ferronato, C.; Salvador, A.; Yang, X.; Chovelon, J.-M. Degradation of Sunscreen Agent 2-Phenylbenzimidazole-5-Sulfonic Acid by TiO_2 Photocatalysis: Kinetics, Photoproducts and Comparison to Structurally Related Compounds. *Appl. Catal. B Environ.* **2013**, *140–141*, 457–467. [CrossRef]
20. Ji, Y.; Zhou, L.; Zhang, Y.; Ferronato, C.; Brigante, M.; Mailhot, G.; Yang, X.; Chovelon, J.-M. Photochemical Degradation of Sunscreen Agent 2-Phenylbenzimidazole-5-Sulfonic Acid in Different Water Matrices. *Water Res.* **2013**, *47*, 5865–5875. [CrossRef]
21. Javidparvar, A.A.; Naderi, R.; Ramezanzadeh, B. Manipulating Graphene Oxide Nanocontainer with Benzimidazole and Cerium Ions: Application in Epoxy-Based Nanocomposite for Active Corrosion Protection. *Corros. Sci.* **2020**, *165*, 108379. [CrossRef]

22. Aljourani, J.; Golozar, M.A.; Raeissi, K. The Inhibition of Carbon Steel Corrosion in Hydrochloric and Sulfuric Acid Media Using Some Benzimidazole Derivatives. *Mater. Chem. Phys.* **2010**, *121*, 320–325. [CrossRef]
23. Ferrari, I.V.; Narducci, R.; Prestopino, G.; Costantino, F.; Mattoccia, A.; Di Giamberardino, L.; Nocchetti, M.; Di Vona, M.L.; Paolone, A.; Bini, M.; et al. Layered Double Hydroxides as a Drug Delivery Vehicle for S-Allyl-Mercapto-Cysteine (SAMC). *Processes* **2021**, *9*, 1819. [CrossRef]
24. Cao, Y.; Dong, S.; Zheng, D.; Wang, J.; Zhang, X.; Du, R.; Song, G.; Lin, C. Multifunctional Inhibition Based on Layered Double Hydroxides to Comprehensively Control Corrosion of Carbon Steel in Concrete. *Corros. Sci.* **2017**, *126*, 166–179. [CrossRef]
25. Yu, J.; Wang, Q.; O'Hare, D.; Sun, L. Preparation of Two Dimensional Layered Double Hydroxide Nanosheets and Their Applications. *Chem. Soc. Rev.* **2017**, *46*, 5950–5974. [CrossRef]
26. Smalenskaite, A.; Vieira, D.E.L.; Salak, A.N.; Ferreira, M.G.S.; Katelnikovas, A.; Kareiva, A. A Comparative Study of Co-Precipitation and Sol-Gel Synthetic Approaches to Fabricate Cerium-Substituted MgAl Layered Double Hydroxides with Luminescence Properties. *Appl. Clay Sci.* **2017**, *143*, 175–183. [CrossRef]
27. Liu, J.; Chen, G.; Yang, J. Preparation and Characterization of Poly(Vinyl Chloride)/Layered Double Hydroxide Nanocomposites with Enhanced Thermal Stability. *Polymer* **2008**, *49*, 3923–3927. [CrossRef]
28. Alibakhshi, E.; Ghasemi, E.; Mahdavian, M.; Ramezanzadeh, B. A Comparative Study on Corrosion Inhibitive Effect of Nitrate and Phosphate Intercalated Zn-Al- Layered Double Hydroxides (LDHs) Nanocontainers Incorporated into a Hybrid Silane Layer and Their Effect on Cathodic Delamination of Epoxy Topcoat. *Corros. Sci.* **2017**, *115*, 159–174. [CrossRef]
29. Pushparaj, S.S.C.; Forano, C.; Prevot, V.; Lipton, A.S.; Rees, G.J.; Hanna, J.V.; Nielsen, U.G. How the Method of Synthesis Governs the Local and Global Structure of Zinc Aluminum Layered Double Hydroxides. *J. Phys. Chem. C* **2015**, *119*, 27695–27707. [CrossRef]
30. Guo, X.; Xu, S.; Zhao, L.; Lu, W.; Zhang, F.; Evans, D.G.; Duan, X. One-Step Hydrothermal Crystallization of a Layered Double Hydroxide/Alumina Bilayer Film on Aluminum and Its Corrosion Resistance Properties. *Langmuir* **2009**, *25*, 9894–9897. [CrossRef]
31. Serdechnova, M.; Salak, A.N.; Barbosa, F.S.; Vieira, D.E.L.; Tedim, J.; Zheludkevich, M.L.; Ferreira, M.G.S. Interlayer Intercalation and Arrangement of 2-Mercaptobenzothiazolate and 1,2,3-Benzotriazolate Anions in Layered Double Hydroxides: In Situ X-ray Diffraction Study. *J. Solid State Chem.* **2016**, *233*, 158–165. [CrossRef]
32. Li, W.; Liu, A.; Tian, H.; Wang, D. Controlled Release of Nitrate and Molybdate Intercalated in Zn-Al-Layered Double Hydroxide Nanocontainers towards Marine Anticorrosion Applications. *Colloid Interface Sci. Commun.* **2018**, *24*, 18–23. [CrossRef]
33. Xu, Z.P.; Braterman, P.S. Synthesis, Structure and Morphology of Organic Layered Double Hydroxide (LDH) Hybrids: Comparison between Aliphatic Anions and Their Oxygenated Analogs. *Appl. Clay Sci.* **2010**, *48*, 235–242. [CrossRef]
34. Liu, A.; Tian, H.; Li, W.; Wang, W.; Gao, X.; Han, P.; Ding, R. Delamination and Self-Assembly of Layered Double Hydroxides for Enhanced Loading Capacity and Corrosion Protection Performance. *Appl. Surf. Sci.* **2018**, *462*, 175–186. [CrossRef]
35. Hu, J.; Gan, M.; Ma, L.; Zhang, J.; Xie, S.; Xu, F.; Shen, J.Z.X.; Yin, H. Preparation and Enhanced Properties of Polyaniline/Grafted Intercalated ZnAl-LDH Nanocomposites. *Appl. Surf. Sci.* **2015**, *328*, 325–334. [CrossRef]
36. Kaghazchi, L.; Naderi, R.; Ramezanzadeh, B. Improvement of the Dual Barrier/Active Corrosion Inhibition Function of the Epoxy Composite Filled with Zinc Doped-Phytic Acid-Modified Graphene Oxide Nanosheets. *Prog. Org. Coat.* **2022**, *168*, 106884. [CrossRef]
37. He, X.; Wu, J.; Li, S.; Chen, Y.; Zhang, L.; Sheng, X. In Situ Growth of Aminated Silica on MXene Nanosheets: A Novel 0D/2D Hybrid Structure for Multifunctional Waterborne Epoxy Composite Coatings. *Prog. Org. Coat.* **2022**, *171*, 107042. [CrossRef]
38. Deip, A.R.; Leal, D.A.; Sakae, G.H.; Maia, F.; Berton, M.A.C.; Ferreira, M.G.S.; Marino, C.E.B. Performance of Commercial LDH Traps for Chloride Ion in a Commercial Corrosion Protection Primer for Petrochemical Industry. *Corros. Eng. Sci. Technol.* **2020**, *55*, 66–74. [CrossRef]
39. Hirschorn, B.; Orazem, M.E.; Tribollet, B.; Vivier, V.; Frateur, I.; Musiani, M. Determination of Effective Capacitance and Film Thickness from Constant-Phase-Element Parameters. *Electrochim. Acta* **2010**, *55*, 6218–6227. [CrossRef]
40. Feng, Y.; Li, H.; Zhang, M.; Jin, J.; Zhang, B.; Wang, Y.; Li, Z. Preparation of BTA@PDA/PANI Microcapsules and Anti-Corrosion Performance of Self-Healing Epoxy Coatings on Low Carbon Steel. *Colloids Surf. Physicochem. Eng. Asp.* **2022**, *649*, 129481. [CrossRef]
41. Huang, H.; Huang, X.; Xie, Y.; Tian, Y.; Jiang, X.; Zhang, X. Fabrication of H-BN-RGO@PDA Nanohybrids for Composite Coatings with Enhanced Anticorrosion Performance. *Prog. Org. Coat.* **2019**, *130*, 124–131. [CrossRef]
42. Xie, Y.; Chen, M.; Xie, D.; Zhong, L.; Zhang, X. A Fast, Low Temperature Zinc Phosphate Coating on Steel Accelerated by Graphene Oxide. *Corros. Sci.* **2017**, *128*, 1–8. [CrossRef]
43. Feng, Z.; Frankel, G.S. Evaluation of Coated Al Alloy Using the Breakpoint Frequency Method. *Electrochim. Acta* **2016**, *187*, 605–615. [CrossRef]
44. Li, S.; Huang, H.; Chen, F.; He, X.; Ma, Y.; Zhang, L.; Sheng, X.; Chen, Y.; Shchukina, E.; Shchukin, D. Reinforced Anticorrosion Performance of Waterborne Epoxy Coating with Eco-Friendly L-Cysteine Modified $Ti_3C_2T_x$ MXene Nanosheets. *Prog. Org. Coat.* **2021**, *161*, 106478. [CrossRef]
45. Cao, Y.; Zheng, D.; Lin, C. Effect of Physical Barrier and Anion-Exchange Process of Nitrate-Intercalated ZnAl Layered Double Hydroxide Films Grown on Al on Corrosion Protection. *Surf. Coat. Technol.* **2021**, *421*, 127436. [CrossRef]

46. Tedim, J.; Kuznetsova, A.; Salak, A.N.; Montemor, F.; Snihirova, D.; Pilz, M.; Zheludkevich, M.L.; Ferreira, M.G.S. Zn–Al Layered Double Hydroxides as Chloride Nanotraps in Active Protective Coatings. *Corros. Sci.* **2012**, *55*, 1–4. [CrossRef]
47. Ning, Y.; Jian, D.; Liu, S.; Chen, F.; Song, Y.; Li, S.; Liu, B. Designing a $Ti_3C_2T_x$ MXene with Long-Term Antioxidant Stability for High-Performance Anti-Corrosion Coatings. *Carbon* **2023**, *202*, 20–30. [CrossRef]
48. Zhang, S.; Hou, L.; Wei, Y.; Du, H.; Wei, H.; Liu, B.; Chen, X. Dual Functions of Chloride Ions on Corrosion Behavior of Mild Steel in CO_2 Saturated Aqueous Solutions. *Mater. Corros.* **2019**, *70*, 888–896. [CrossRef]